Supplementary Material online

Population genomics in Bacteria: A case study of *Staphylococcus aureus*

Shohei Takuno, Tomoyuki Kado, Ryuichi P. Sugino, Luay Nakhleh & Hideki Innan

Contents

1 Estimating recombination rate

In eukaryotes, it is a common approach to estimate the recombination rate from the decay of linkage disequilibrium against distance. This approach usually requires a sample size > 4, but Ruderfer et al. (2006) recently developed a new method that uses a population sample with size 3 and an outgroup. We applied this method to the A-B-C trio assuming D and E as outgroups. Ruderfer et al. (2006) 's method focuses on the compatibility of the coalescent patterns at a pair of variable sites. In our analysis, we used 5,289 SNPs at which the allelic configuration of {A, B, C, D, E} $\in \{\{1,1,0,0,0\},\{0,1,1,0,0\},\{1,0,1,0,0\}\}$, where 0 and 1 represent two variable nucleotides. For these sites, it is very likely that 0 is the ancestral allelic state; therefore, the tree shape can be parsimoniously inferred (*i.e.,* ((A, B), C), ((B, C), A) and ((A, C), B) are given for $\{1,1,0,0,0\}$, $\{0,1,1,0,0\}$, and $\{1,0,1,0,0\}$, respectively). It is expected that the probability of tree-shape compatibility for a pair of completely linked sites is 1 and this probability decreases as the recombination rate between the two sites increases. When the two sites are completely unlinked, the probability is 1/3. Thus, the decrease of the probability of tree-shape compatibility against distance is analogous to the decay of LD (see fig. 5*B* in the main article).

We used coalescent simulations to determine what recombination parameter gives a good fit to the observed decay of the probability of tree-shape compatibility. The simulation was performed by using Hudson's ms software (Hudson 2002), assuming a constant-size panmictic population. As mentioned in the main article, bacterial homologous recombination events should have similar outcome to that of allelic gene conversion rather than crossing over in eukaryotes (Didelot and Falush 2007, Wiuf and Hein 2000). Therefore, we set the crossing-over rate = 0 in ms, and investigated how allelic gene conversion alone could explain the observed decay of the probability of tree-shape compatibility. The model of gene conversion in the ms software involves two parameters, the initiation rate of gene conversion event per bp per population, $G = 2Ng$, where g is initiation rate of an event per adjacent sites and N is effective population size, and the average length of gene conversion tract $(1/q)$ (Hudson 2002). Tract length, z, is assumed to be a random variable from a geometric distribution: $q(1-q)^{z-1}$ (Wiuf and Hein 2000). This gene conversion model has been well incorporated in the coalescent process of bacterial populations to simulate

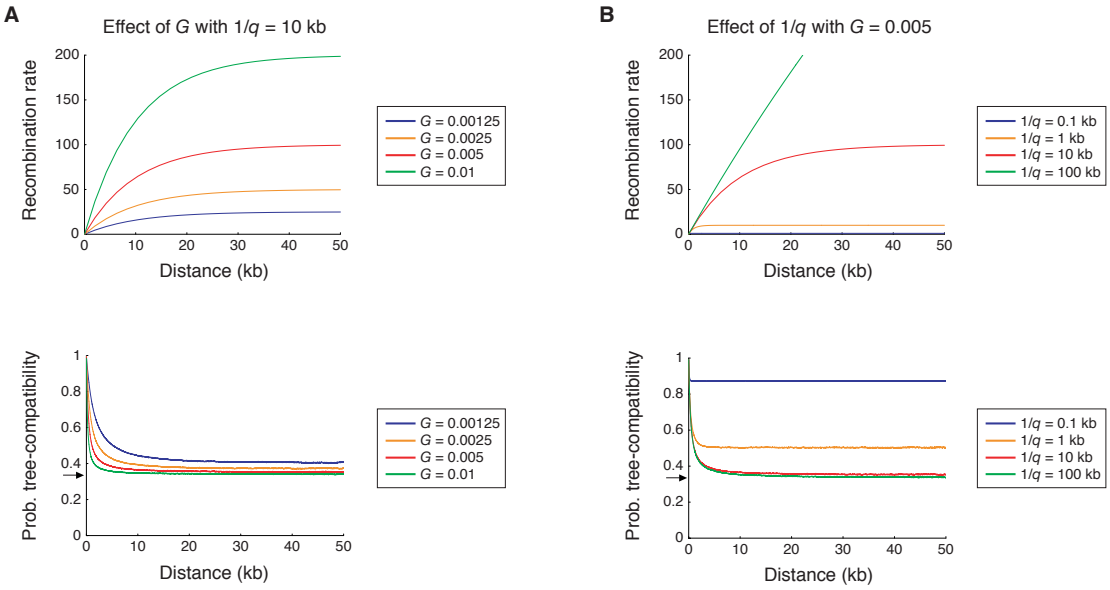

Supplementary Fig. S1. Effects of the initiation rate of a homologous recombination event (*G*) and tract length (1/*q*). The *x*-axes represents distance between SNPs. The *y*-axes in the upper and lower panels represent *R* (defined by equation (1)) and probability of tree-shape compatibility, respectively. (*A*) The effect of *G*. The tract length of gene conversion (1/*q*) is fixed to be 10 kb. (*B*) The effect of 1/*q*. *G* is fixed to be 0.005.

homologous recombination (Didelot and Falush 2007).

The theoretical relationship between the recombination rate, R, and the gene conversion parameters, G and q, is relatively simple: R for a pair of sites with distance d bp is given by

$$R = 2G\,\frac{1}{q}\,(1 - e^{-\frac{d}{1/q}}), \tag{1}$$

according to Langley *et al.* (Langley et al. 2000). This equation means that R increases with increasing d, and R will saturate at $R = 2G/q$ when $d \gg 1/q$. Then, the probability of tree-shape compatibility is determined by R. The probability is 1 with $R = 0$, and when R is sufficiently large the probability is close to the theoretical minimum, 1/3.

Supplementary fig. S1 demonstrates the effects of G and q on R and the tree-shape compatibility, obtained by coalescent simulations with wide ranges of G and $1/q$. In Supplementary fig. S1*A*, the effect of G is shown by fixing $1/q$ = 10 kb, indicating the major effect of G is to determine the slope of R and the probability of tree-shape compatibility. Supplementary fig. S1*B* is to show the effect of $1/q$ by fixing G = 0.005. As expected from equation (1), $1/q$ determines the upper limit of R and the lower limit of the probability of

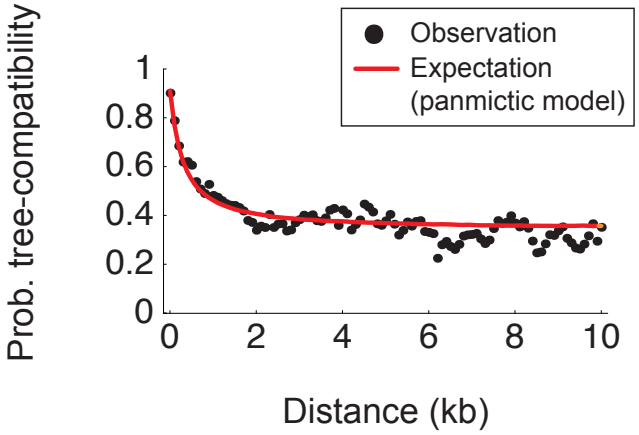

Supplementary Fig. S2. Expected decay of the probability of tree-compatibility with the estimated G and $1/q$.

tree-shape compatibility. R and the probability of tree-shape compatibility saturate when $d \gg 1/q$

Thus, because the decay of the probability of tree-shape compatibility can be well characterized by G and $1/q$, it is possible to estimate these parameters from the observation. We further performed simulations with wide ranges of G and $1/q$, and the fit of the simulated decay to the observation was examined by the least-square method. It was found that best fits were obtained when $\hat{G} = 0.007$ and $\hat{1/q} \geq 10$ kb. As an estimate of θ is 0.0156, we have an estimate of the ratio of G to θ (or the ratio of g to μ) to be 0.45. These estimated parameters provide an excellent fit to the observation (Supplementary fig. S2).

2 Inferring demographic history

The demographic history of the A-B-C trio was inferred according to the theories of Takahata, Satta, and Klein (1995) and Hudson (1983) (see also Wu (1991) and Chen and Li (2001)). Based on our observations (see the main article), we considered that the ancestral lineages of the three groups should have shared a large ancestral population. Considering that the proportion of the ((A, B), C) tree is slightly higher than the other two, we presumed a model as illustrated in fig. 6A. The ancestral population with size N_2 first split into two populations at time t_2, and one of them with size N_1 further split into two at time t_1. It was assumed that the Wright-Fisher model for a haploid species is applied to each population.

First, N_2 and t_2 were estimated by using the theory of Takahata, Satta, and Klein (1995). The results for the divergence data between A and C are shown here (essentially the same result is expected for the B-C pair). In practice, this theory is to divide the divergence between a pair of sequences into two components: that due to the accumulation of mutations after the population split (*i.e.,* after t_2), and that due to mutations occurred in the coalescent process in their ancestral population (*i.e.*, before t_2). The expectations of these two components are given by μt_2 and $\theta_2 = 2N_2\mu$, respectively, so that we can estimate N_2 and t_2 given μ, where μ is the mutation rate per site per generation.

Takahata, Satta, and Klein (1995)'s theory provides maximum likelihood (ML) estimates of μt_2 and θ_2 from divergence data in multiple independent regions, within which no recombination is assumed. Therefore, we applied this theory to synonymous nucleotide divergences of 1,071 genes, where no intragenic recombination was detected by Hudson and Kaplan (1985)'s four-gamete test. Because we observed gene-by-gene changes of the tree shape of A-B-C in fig. 2*C*, we ignored the linkage between investigated genes. Theoretically, when neighbor genes are partially linked (but treated independently), there is very little effect on the ML estimates if the number of genes is sufficiently large, although the confidence intervals of the ML estimates will be underestimated. Following Takahata, Satta, and Klein (1995), let k_i and n_i be the number of synonymous differences and sites at the ith gene. m is the number of total genes (*i.e.,* m = 1,071). Then, the log-likelihood function of the observation of $K = \{k_1, k_2 \ldots, k_m\}$ is given by

$$LL_1(\theta_2, \mu t_2 | K) = \sum_{i=1}^{m} \ln[(1 - a_{i2})\ a_{i2}^{k_i}\ e^{-2b_{i2}}\ c(k_i; 2b_{i2}, a_{i2})], \tag{2}$$

where

$$a_{i2} = \theta_2 n_i / (1 + \theta_2 n_i) \tag{3}$$

$$b_{i2} = \mu t_2 n_i \tag{4}$$

and

$$c(k; b, a) = \sum_{j=0}^{k} \frac{1}{j!} \left(\frac{b}{a}\right)^j. \tag{5}$$

By using this equation, we obtained ML estimates of $\hat{\theta}_2$ and $\mu\hat{t}_2$ (estimated parameters are shown with a hat) to be $\hat{\theta}_2 = 0.0107$ and $\mu\hat{t}_2 = 0.000356$, indicating that the population split occurred very recently. t_2 is only 7 % of the expected coalescent time (N_2) in the ancestral population. We confirmed that almost identical results were obtained by using the divergence between B and C; ML estimates were $\hat{\theta}_2 = 0.0103$ and $\mu\hat{t}_2 = 0.000351$.

We next estimated $\theta_1 = 2N_1\mu$ and μt_1 conditional on the ML estimates $\hat{\theta}_2 = 0.0105$ and $\mu\hat{t}_2 = 0.000354$, which are the average of the estimates for the A-C and B-C pairs. In this step, we first focused on the proportion of the three possible tree shapes, ((A, B), C), ((B, C), A) and ((A, C), B). In our observation (fig. 2*B*), the proportion of ((A, B), C) is slightly higher than those of ((B, C), A) and ((A, C), B) (40.8 vs. 28.4 and 30.8 %), from which $\theta_1 = 2N_1\mu$ and μt_1 can be estimated (Chen and Li 2001, Hudson 1983, Wu 1991). Here, we define

$$T = (t_2 - t_1)/N_1, \tag{6}$$

then we can estimate T as $\hat{T} = -\ln[(3/2)(1 - P_{((A,B),C)})] = 0.119$ because $P_{((A,B),C)} = 1 - e^{-2T/3}$ (Chen and Li 2001, Hudson 1983, Wu 1991). However, T is a function of N_1 and μ, and it is desired to estimate them separately. To do so, we developed an ML function of the observed synonymous divergence between A and B by modifying Equation (2) as described below.

Let k_i and n_i be the number of synonymous differences and sites at the ith gene. The likelihood function of k_i was obtained by considering the two patterns of the coalescent; (i)

the two lineages coalesce between t_1 and t_2, and (ii) the coalescent event predates t_2. The probabilities of the two alternative patterns are given by $1 - e^{-\hat{T}}$ and $e^{-\hat{T}}$, respectively.

In the former case (i), the likelihood function of k_i is given by

$$P_1(k_i) = \frac{1}{1 - e^{-\hat{T}}} \, (1 - a_{i1}) \, a_{i1}^{k_i} \, [e^{-2b_{i1}} \, c(k_i; 2b_{i1}, a_{i1}) - e^{-\hat{T}} \, e^{-2b_{i2}} \, c(k_i; 2b_{i2}, a_{i1})], \quad (7)$$

where

$$a_{i1} = \theta_1 n_i / (1 + \theta_1 n_i) = f(\mu t_1) n_i / (1 + f(\mu t_1) n_i), \quad (8)$$

$$f(\mu t_1) = \frac{2(\mu \hat{t}_2 - \mu t_1)}{\hat{T}} \quad (9)$$

and

$$b_{i1} = \mu t_1 n_i. \quad (10)$$

In the latter case (ii), the function is identical to Equation (2):

$$P_2(k_i) = (1 - a_{i2}) \, a_{i2}^{k_i} \, e^{-2b_{i2}} \, c(k_i; 2b_{i2}, a_{i2}). \quad (11)$$

Then, from (7)-(11), we have the unconditional probability:

$$P(k_i) = (1 - e^{-\hat{T}}) P_1(k_i) + e^{-\hat{T}} P_2(k_i) \, , \quad (12)$$

and the log-likelihood function for the entire data is given by

$$LL_2(\mu t_1 | K) = \sum_{i=1}^{m} \ln P(k_i) \, . \quad (13)$$

We obtained an ML estimate of $\mu \hat{t}_1$ to be 0, so that $\hat{\theta}_1 = 0.00597 = 0.569 \hat{\theta}_2$ from equation (13).

3 Estimating recombination rate under the inferred demography

The previous section suggest that it would be more appropriate to used the inferred demography rather than assuming a complete panmictic model for the A-B-C trio. We repeated the same coalescent simulation analysis with Hudson's ms software (Hudson 2002), where we assumed the demography estimated in the previous section. It was found that best fits were obtained when $\hat{G} = 0.006$ and $\hat{1/q} \geq 10$ kb. As an estimate of θ is 0.105, we have an estimate of the G/θ (or g/μ) ratio to be 0.6, which is slightly higher than that obtained assuming a panmictic model. The results are shown in fig. 6 in the main article.

4 Effect of recombination from external source on the elevation of LD

It is theoretically true that recombination from external source can elevate local LD, as illustrated in Supplementary fig. S3, where typical patterns of informative sites in the alignment of the A-B-C trio and an outgroup (E or D) are shown. In a clonal model allowing recombination with external source, recombinational events would be classified essentially into two types. For our analysis of the A-B-C trio, external sources could be not only the outgroups (D and E) but also any other bacterial strains including other species. One type is recombinations that occurred between one of the A-B-C trio and a random external source (referred to as type I recombination), and the other (referred to as type II recombi-

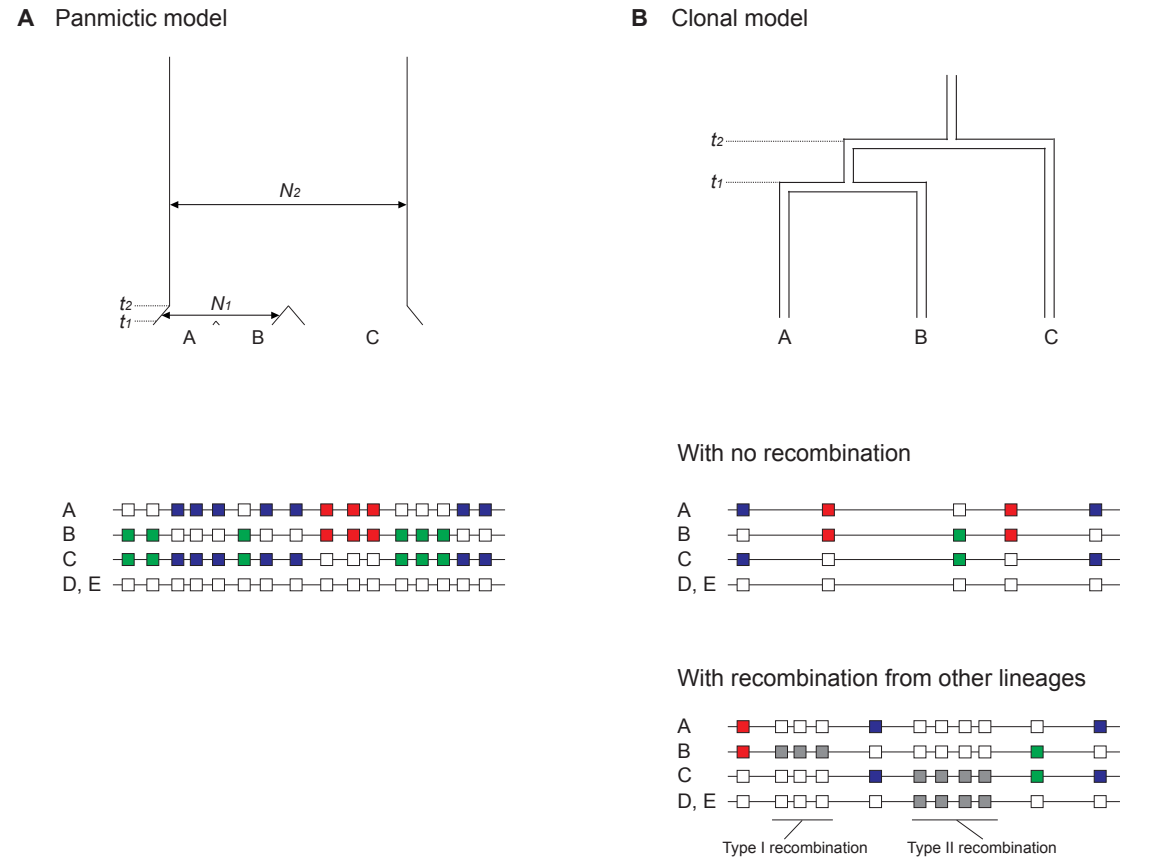

Supplementary Fig. S3. Illustrating typical patterns of SNPs under a panmictic model with homologous recombination (A) and clonal model without and with recombination between external source (B).

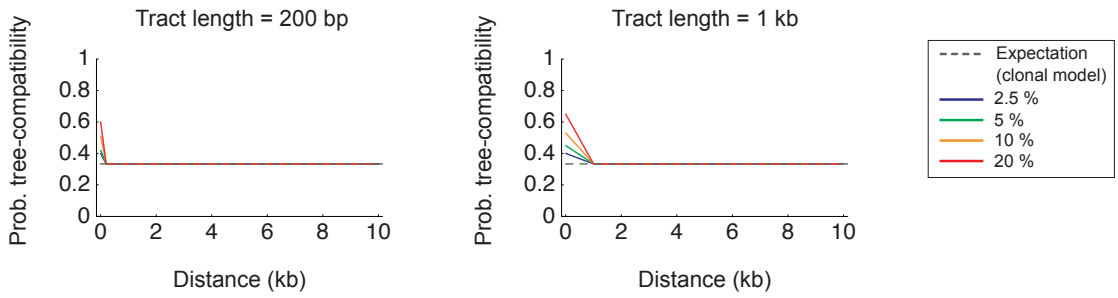

Supplementary Fig. S4. The expected decay of LD (probability of tree-incompatibility) under a clonal model with recombination between external source (Supplementary fig. S3B). The average tract length of homologous recombination was fixed to be 200 bp in the left panel, which is the average of regions with clear signature of recombination with external sources in our data. We observe an elevation of LD (tree-compatibility) up to 200 bp. The length was changed to 1 kb in the right panel. The region with elevated LD is extended to 1 kb.

nation) is a special case where the external source happened to be the outgroup (E or D). It is important to notice that only type II recombinations can create informative sites so that our analysis could be potentially affected. As illustrated in Supplementary fig. S3B, type I recombination introduces only singletons.

To address how much this level of type II recombination can elevate LD, we repeated the same simulation under the clonal model, except that a certain rate of type II recombination is allowed. The recombination rate was adjusted such that $\{2, 5, 10, 20\}\%$ of the genome has the tree shapes supporting type II recombination, and the expected decay of LD (probability of tree-compatibility) was obtained. Supplementary fig. S4 shows that the effect to elevate local LD is quite small; even when 10% of the genome experienced recent type II recombination, LD for very short distances is increased only to 0.5.

It should be noted that this theoretical analysis was performed to see how regions with recombination from external sources contribute to the decay of LD if those regions are included. LD is indeed decreased, but this does not apply to our LD analysis in the main article because such regions were excluded in the analysis.

5 References

Chen FC, Li WH. 2001. Genomic divergences between humans and other hominoids and the effective population size of the common ancestor of humans and chimpanzees. Am. J. Hum. Genet. 68:444–456.

Didelot X, Falush D. 2007. Inference of bacterial microevolution using multilocus sequence data. Genetics 175:1251–1266.

Hudson RR. 1983. Testing the constant-rate neutral allele model with protein sequence data. Evolution 37:203–217.

Hudson RR. 2002. Generating samples under a Wright-Fisher neutral model of genetic variation. Bioinformatics 18:337–338.

Hudson RR, Kaplan NL. 1985. Statistical properties of the number of recombination events in the history of a sample of DNA sequences. Genetics 111:147–164.

Langley CH, Lazzaro BP, Phillips W, Heikkinen E, Braverman JM. 2000. Linkage disequilibria and the site frequency spectra in the *su(s)* and *su(w(a))* regions of the *Drosophila melanogaster* X chromosome. Genetics 156:1837–1852.

Ruderfer DM, Pratt SC, Seidel HS, Kruglyak L. 2006. Population genomic analysis of outcrossing and recombination in yeast. Nat. Genet. 38:1077–1081.

Takahata N, Satta Y, Klein J. 1995. Divergence time and population size in the lineage leading to modern humans. Theor. Popul. Biol. 48:198–221.

Wiuf C, Hein J. 2000. The coalescent with gene conversion. Genetics 155:451–462.

Wu CI. 1991. Inferences of species phylogeny in relation to segregation of ancient polymorphisms. Genetics 127:429–435.